Supporting Information
for
New mechanistic insight into intramolecular arene hydroxylation initiated by (μ-1,2-peroxo)diiron(III) complexes with dinucleating ligands

Mio Sekino, Hideki Furutachi, Kyosuke Tasaki, Takanao Ishikawa, Shigeki Mori, Shuhei Fujinami, Shigehisa Akine, Yoko Sakata, Takashi Nomura, Takashi Ogura, Teizo Kitagawa, and Masatatsu Suzuki

Contents:

Figure S1.	An ORTEP view of [Fe$_2$(OH)$_2$(H-L)]$^{2+}$ (**1**-H) with a full numbering scheme of atoms. Hydrogen atoms are omitted for clarity.
Table S1.	Selected bond distances (Å) and angles (deg) of **1**-H.
Figure S2.	An ORTEP view of [Fe$_2$(OH)$_2${H(H-L-O)}$_2$]$^{4+}$ (**3**-H) with a full numbering scheme of atoms. Hydrogen atoms are omitted for clarity.
Table S2.	Selected bond distances (Å) and angles (deg) of **3**-H.
Figure S3.	Electronic spectra of (a) **2**-tBu (black) and its decomposition species (red) (b) **2**-NO$_2$ (black) and its decomposition species (red) in acetone at –20°C.
Figure S4.	Resonance Raman spectra of **2**-H generated in the reaction of **1**-H with ^{16}O$_2$ (black) and ^{18}O$_2$ (blue) in d$_6$-acetone at –40 °C with a 647.1 nm laser excitation.
Figure S5.	ESI-TOF mass spectra of samples obtained by the decomposition of (a) **2**-H, (b) **2**-tBu, and (c) **2**-NO$_2$.
Figure S6.	NMR specta of (a) a sample obtained by the decomposition of **2**-H, (c) its 6 – 8 ppm region, (b) H-L-H in 6 – 8 ppm region in CDCl$_3$. IS is an internal standard (2,6-dimetyl-1,4-benzoquinone). The asterisked signal is CHCl$_3$. Yield of H-L-OH was estimated by the average values obtained by comparison of the integrated area of the signals of 8, 4, and 1 with that of IS.
Figure S7.	NMR specta of (a) a sample obtained by the decomposition of **2**-*t*Bu, (c) its 6 – 8 ppm region, (b) *t*Bu-L-H in 6 – 8 ppm region in acetone-*d*$_6$. IS is an internal standard (2,6-dimetyl-1,4-benzoquinone). The asterisked signal is CHCl$_3$. Yield of *t*Bu-L-OH was estimated by the average values obtained by comparison of the integrated area of the signals of 8, 4, and 1 with that of IS.
Figure S8.	NMR spectra of (a) a sample obtained by the decomposition of **2**-NO$_2$, (c) its 6.5 – 8.5 ppm region, (b) NO$_2$-L-H in 6.5 – 8.5 ppm region in CDCl$_3$. IS is an internal standard (2,6-dimetyl-1,4-benzoquinone). The asterisked signal is CHCl$_3$. Yield of NO$_2$-L-OH was estimated by the average values obtained by comparison of the integrated area of the signals of 8, 4, and 1 with that of IS.
Figure S9.	Yield of (a) hydroxylated ligands (tBu-L-OH, H-L-OH, and NO$_2$-L-OH) and (b) acetic acid.
Figure S10.	ESI-TOF mass spectra of red solution decomposed by **2**-H in (a) acetone and (b) d$_6$-acetone at −20 °C.
Figure S11.	GC-mass spectra of acetic acid obtained in the decomposition of **2**-H in (a) acetone and (b) d$_6$-acetone.
Figure S12.	Representative electronic spectral changes for decompositions of (a) **2**-H ([**2**-H] = 1.14 mM), (b) **2**-*t*Bu ([**2**-*t*Bu] = 1.44 mM), and (c) **2**-NO$_2$ ([**2**-

NO_2] = 1.02mM) in acetone at −20 °C. Insets are the decay-time profile of the absorbance at 700 nm (curve) and the pseudo-first-order plot (linear plot). (d) Hammet plot for the decomposition of **2**-R in acetone at −20 °C. Solid line represents a least square fit with the slope $\rho = 0.014$.

Figure S13. Eyring plots for decompositions of **2**-R (R = H, *t*Bu and NO_2) in acetone.

Table S3. The First Order Rate Constants (*k*) for the Decomposition Reactions of **2**-R (R = H, *t*Bu and NO_2) in acetone. Deviation of the *k* value were estimated within 10%.

Table S4. Kinetic Activation Parameters for the Decomposition Reactions of **2**-R (R = H, *t*Bu and NO_2) in acetone.

Figure S14. ESI-TOF mass spectra of (a) a sample obtained by the decomposition of **2**-H prepared from $^{16}O_2$, (b) a sample obtained by the decomposition of **2**-H prepared from $^{18}O_2$, and (c) a sample obtained by the decomposition of **2**-H prepared from $^{16}O_2$ in the presence of 1000 eqiv. of $H_2{}^{18}O$ at −20 °C.

Materials. Acetone and d$_6$-acetone were dried over $CaSO_4$ and distilled under N_2 before use. THF was distilled from sodium/benzophenone under N_2. Acetonitrile was dried over CaH_2 and distilled under N_2. $^{18}O_2$ (95% ^{18}O-enriched) and $H_2{}^{18}O$ (≧98% ^{18}O-enriched) were purchased from TAIYO NIPPON SANSO Corporation (Tokyo, Japan). 1,3-Bis[bis(6-methyl-2-pyridylmethyl)aminomethyl]benzene (H-L), 1,3-bis[bis(6-methyl-2-pyridylmethyl)aminomethyl]-5-*tert*-butylbenzene (*t*-Bu-L), and 1,3-Bis[bis(6-methyl-2-pyridylmethyl)aminomethyl]-5-nitrobenzene (NO_2-L) were synthesized according to the literature methods (T. Mastumoto, *J. Am. Chem Soc.* **2006**, *128*, 3874-3875). $Fe(CF_3SO_3)_2\cdot 2MeCN$ was synthesized according to the literature method (K. S. Hagen, *Inorg. Chem.* **2000**, *39*, 5867-5869). $Fe(CF_3SO_3)_2$ was purchased from Wako Pure Chemical Industries LTD (Japan). All other reagents and solvents were commercially available and used without further purification.

Syntheses of Complexes. Diiron(II) complexes were prepared under N_2 using a grove box (Miwa MFG Co., LTD, Model DBO-1B) or by standard Schlenk techniques.

[Fe$_2$(OH)$_2$(H-L)](CF$_3$SO$_3$)$_2$ (1-H). A THF solution (6 mL) of $Fe(CF_3SO_3)_2\cdot 2MeCN$ (436 mg, 1 mmol) was added to a THF solution (5 mL) of H-L (278 mg, 0.5 mmol) to give a yellow solution, to which was added dropwise a THF solution (3 mL) containing H_2O (18 μL, 1 mmol) and triethylamine (138 μL, 1 mmol) with stirring to give a pale green powder. The pale green powder was filtered and washed with THF. Yield: 0.489 g (77%). Single crystals of **1**-H suitable for X-ray crystallography were obtained by slow diffusion of diethyl ether onto a dichloromethane solution of **1**-H. ESI-MS (in acetone): *m/z* (relative intensity): 342.1 (100) $[Fe_2(O)(H\text{-}L)]^{2+}$, 351.1 (70) $[Fe_2(OH)_2(H\text{-}L)]^{2+}$. UV-Vis [$\lambda_{max}$/nm ($\varepsilon$/M^{-1} cm^{-1})] in acetone at −20 °C: 330 (1000). Anal. Calcd for $C_{38}H_{42}F_6Fe_2N_6O_8S_2$: C, 45.61; H, 4.23; N, 8.40 %. Found: C, 45.52; H, 4.25; N, 8.66 %.

[Fe$_2$(OH)$_2$(*t*Bu-L)](CF$_3$SO$_3$)$_2$·H$_2$O·THF (1-*t*Bu). To a suspension of $Fe(CF_3SO_3)_2$ (353 mg, 1 mmol) in acetonitrile (2 mL) was added *t*Bu-L (306 mg, 0.5 mmol) in acetonitrile (2 mL) to give a pale brown solution. The resulting solution was allowed to stand for several days under vapor of diethyl ether to give colorless crystals of $[Fe_2(t\text{-}Bu\text{-}L)](CF_3SO_3)_4\cdot 4CH_3CN\cdot 2H_2O$ (Anal. Calcd for $C_{48}H_{56}F_{12}Fe_2N_{10}O_{14}S_4$: C, 41.06; H, 4.24; N, 9.21 %. Found: C, 41.04; H, 4.50; N, 9.20 %.). The colorless crystals (190 mg, 0.125 mmol) were dissolved in THF (4 mL), to which was added dropwise a THF solution (3 mL) containing triethylamine (34 μL, 0.25 mmol) with stirring to give a pale green powder. The pale green powder was filtered, washed with THF. Yield: 0.090 g (68 %). ESI-MS (in acetone): *m/z* (relative intensity): 370.1 (100) $[Fe_2(O)(t\text{-}Bu\text{-}L\text{-}H)]^{2+}$, 379.1 (90) $[Fe_2(OH)_2(tBu\text{-}L\text{-}H)]^{2+}$. UV-Vis [$\lambda_{max}$/nm ($\varepsilon$/M^{-1} cm^{-1})] in acetone at −20 °C: 330 (1000). Anal. Calcd for $C_{46}H_{60}F_6Fe_2N_6O_{10}S_2$: C, 48.18; H, 5.27; N, 7.33 %. Found: C, 48.38; H, 5.20; N, 7.46 %.

[Fe$_2$(OH)$_2$(NO$_2$-L)](CF$_3$SO$_3$)$_2$·4H$_2$O (1-NO$_2$). To a suspension of $Fe(CF_3SO_3)_2$ (353 mg, 1 mmol) in acetonitrile (2 mL) was added NO_2-L (306 mg, 0.5 mmol) in acetonitrile (2 mL) to give a yellow solution. The yellow solution was allowed to stand for several days under vapor of diethyl ether to give yellow crystals of $[Fe_2(NO_2\text{-}L)](CF_3SO_3)_4\cdot 2.5CH_3CN\cdot 2H_2O$ (Anal. Calcd for $C_{45}H_{50.5}F_{12}Fe_2N_{9.5}O_{16}S_4$: C, 37.32; H, 3.51; N, 9.19 %. Found: C, 37.24; H, 3.59; N, 9.46 %.). The yellow crystals (181 mg, 0.125 mmol) were dissolved in THF (4 mL), to which was added dropwise a THF solution (3 mL) containing triethylamine (34 μL, 0.25 mmol) with stirring to give a pale green powder. The pale green powder was filtered, washed with THF. Yield: 0.090 g (68 %). ESI-MS (in acetone): *m/z* (relative intensity): 373.6 (100) $[Fe_2(OH)_2(NO_2\text{-}L)]^{2+}$, 364.6 (40) $[Fe_2(O)(NO_2\text{-}L)]^{2+}$. UV-Vis [$\lambda_{max}$/nm ($\varepsilon$/M^{-1} cm^{-1})] in acetone at −20 ºC: 330 (2200). Anal. Calcd for $C_{38}H_{49}F_6Fe_2N_7O_{14}S_2$: C, 40.84; H, 4.42; N, 8.77 %. Found: C, 40.54; H, 4.15; N, 8.59 %.

$[Fe_2(OH)_2\{H(H\text{-}L\text{-}O)\}_2](CF_3SO_3)_4\cdot 4H_2O$ (3-H). An acetone solution (20 mL) of **1**-H (41 mg, 0.04 mmol) was oxygenated at room temperature and allowed to stand for 3 days at room temperature to give evaporate acetone, the residue was dissolved into acetone (5 mL). The insoluble brown precipitate was filtered, purple solution was allowed to stand for several days under vapor of diethyl ether to give purple crystals. Yield: 3.6 mg (5%). IR (KBr, cm^{-1}): 3377(O-H), 1608 (C=C, aromatic), 1578 (C=C, aromatic), 1279 ($CF_3SO_3^-$), 1160 ($CF_3SO_3^-$). ESI-MS (in acetone): *m/z* (relative intensity): 794.2 (100) $\{[Fe_2(OH)_2(H(H\text{-}L\text{-}O))_2](CF_3SO_3)_2\}^{2+}$, 322.6 (60) $[Fe_2(OH)_2\{H(H\text{-}L\text{-}O)\}_2]^{4+}$. UV-Vis [$\lambda_{max}$/nm ($\varepsilon$/M^{-1} cm^{-1})] in acetone at 25 ºC: 560 (1450). Anal. Calcd for $C_{76}H_{90}F_{12}Fe_2N_{12}O_{20}S_4$: C, 46.58; H, 4.63; N, 8.58 %. Found: C, 46.66; H, 4.33; N, 8.40 %.

Determination of the Molar Extinction Coefficient of $[Fe_2(OH)_2(R\text{-}L)]^{2+}$ (1-R). Since it was difficult to weigh the amounts of **1**-H, **1**-*t*Bu, and **1**-NO$_2$ due to their instability under air, the molar extinction coefficients (ε) of **1**-H, **1**-*t*Bu, and **1**-NO$_2$ were determined as follows. Typically, an appropriate amount of **1**-H was dissolved into acetone (20 mL) and an aliqot (1mL) of this solution was taken up. To the aliqot was added 1,10-phenanthroline (~50 equiv. 10 mg, 0.05 mmol), ascorbic acid (99%, ~50 equiv. 8.8 mg, 0.05 mmol) and water (10 mL) to generate $[Fe^{II}(phen)_3]^{2+}$, and was diluted to 25 mL in the volumetric flask by addition of water, where pH was adjusted to ca. 5 by addition of acetic acid. Then iron concentration was determined spectrophotometrically from the absorbance at 510 nm (the molar extinction coefficient of $[Fe^{II}(phen)_3]^{2+}$ is 1.14×10^4 M^{-1} cm^{-1} at pH = 5).

Identification and Quantification of Modified Ligands by Thermal Decomposition of $[Fe_2(O)(O_2)(R\text{-}L)]^{2+}$ (2-R). Ligand recovery experiments were performed as follows. Typically, an acetone solution (1 mM, 40 mL) of **1**-H was oxygenated at −20 °C and allowed to stand for 24 hours. After acetone was evaporated under reduced pressure, the residue was dissolved into $CHCl_3$ (20 mL) under N_2. To this $CHCl_3$ solution was added an aqueous solution (20 mL) containing 100 equiv. of Na_4edta and NaCl, and the resulting mixture was stirred for 1 hour. After separation of $CHCl_3$ layer, the separated $CHCl_3$ layer was washed with an aqueous solution (20 mL) containing 100 equiv. of Na_4edta and NaCl (two times). The $CHCl_3$ layer separated was washed with an aqueous solution (20 mL) containing 100 equiv. of Na_4edta, 50 equiv. of $Na_2S_2O_4$, and NaCl and the resulting mixture was stirred for 2 hour. After separation of $CHCl_3$ layer, the $CHCl_3$ solution was dried over Na_2SO_4. After filtration, $CHCl_3$ was evaporated under reduced pressure to give an oil. The reaction products were determined by ^{1}H NMR and ESI-TOF/MS, and their amounts were determined by ^{1}H NMR by addition of $CDCl_3$ or d_6-acetone solution containing appropriate amount of 2,6-dimethyl-1,4-benzoquinone as an internal standard (see Figures S4, S5, and S6 for H-L-OH, *t*Bu-L-OH, and NO_2-L-OH, respectively). Total amounts of R-L and R-L-OH recovered were more than 95% for three experiments. Yields of H-L-OH, *t*-Bu-L-OH, and NO_2-L-OH were ~26%, ~32%, and ~8%, respectively.

Identification and Quantification of Acetic acid by Thermal Decomposition of $[Fe_2(O)(O_2)(R\text{-}L)]^{2+}$ (2-R). (a) Identification of acetic acid by GC-MS was performed as follows. Typically, an acetone or d_6-acetone solution (1 mM, 20 mL) of **1**-H was oxygenated at −20 °C and allowed to stand for 24 hours. After acetone was evaporated under reduced pressure, the residue was dissolved into aqueous solution of sulfuric acid (0.3 M, 5 ml). The resulting aqueous solution was heated at 120 °C, and acetic acid was collected by trapping with liquid nitrogen under reduced pressure, which was confirmed by GC-MS (Figure S11): *m/z* (relative intensity): 43.1 (100) $\{CH_3CO\}^+$, 60.1 (84) $\{CH_3COOH\}^+$, 45.1 (83) $\{COOH\}^+$ for acetone sample; 45.1 (100) $\{COOH\}^+ + \{CHD_2CO\}^+$, 46.1 (49) $\{CD_3CO\}^+$, 63.1 (32) $\{CD_3COOH\}^+$ for d_6-acetone sample.

(b) Quantification of acetic acid by ^{1}H NMR was performed as follows. An acetone solution (1 mM, 40 mL) of **1**-H was oxygenated at −20 °C and allowed to stand for 24 hours. After acetone was evaporated under reduced pressure, the residue was dissolved into $CDCl_3$ (1 mL) and D_2O (1 mL), to which was added sodium dithionite (140 g, 0.08mmol) and potassium cyanide (46 mg, 0.72 mmol). After the resulting mixture was stirred for 1 hour, D_2O layer was separated. Amount of acetic acid was determined by ^{1}H NMR by addition of appropriate amount of sodium 2,2-dimethyl-2-silapentate-5-sulfonate (DSS) as an internal standard to separated D_2O layer. Yields of acetic acid for **2**-H, **2**-*t*Bu, and **2**-NO_2 were ~36%, ~40%, and ~37%, respectively.

^{18}O Labeling Experiments. Hydroxylation of ligand H-L was also carried out using $^{18}O_2$ or added $H_2{}^{18}O$. The procedure was the same as that of $^{16}O_2$ experiment except for using $^{18}O_2$. An acetone solution (1 mL) containing 1000 eqiv of $H_2{}^{18}O$ was added to an acetone solution of **2**-H (1 mM, 5 mL). Formation of H-L-^{18}OH was identified by ESI-MS (see Figure S3).

Physical Measurements. Electronic spectra were measured with an Otsuka Electronics photodiode array spectrometer MCPD-2530 with an Otsuka Electronics optical fiber attachment, and Shimazu diode array spectrometer Multispec-1500. The temperatures were controlled by an EYELA low temp. pair stirrer PSL-1800. IR spectra were obtained on the KBr disks with a JASCO FT/IR-4200 spectrometer. Resonance Raman spectra were obtained with a liquid nitrogen cooled CCD detector (400B/LN, Roper Scientific) attached to a polychrometor (Chromex, 500IS equipped with a 1,200 grooves/nm grating). The Kr^+ laser (Model 2016, Spectra Physics) was used as the exiting source (647.1 nm). The laser power used were ~ 20 mW at the sample points. All measurements (135° backscattering geometry) were carried out with a spinning cell (1000 rpm) kept at −40 °C by flushing cold N_2 gas. Raman shifts were calibrated with indene and the accuracy of the peak positions of the Raman bands was ± 1 cm^{-1}. ESI-TOF/MS were measured with a Micromass LCT spectrometer. GC-MS analysis was performed on a Shimadzu GCMS-QP2010 plus. GC-MS instrument equipped with a fused slilica capillary column (100% dimethylpolysiloxane, 0.32 mm diameter × 25 m, QUADREX Corp.). ^1H NMR spectra were measured with JEOL LNM-LM400 using tetramethylsilane (TMS) or sodium 2,2-dimethyl-2-silapentane- 5-sulfonate (DSS) as the internal standard.

Kinetic Measurements. The decompositions of **2**-R in acetone at low temperature under O_2 were followed by UV-Vis spectral changes, which were obtained with an optical fiber (light path length = 0.986 cm) as described in physical measurements. Typical experiment is as follows. An acetone solution of **1**-R (1 mM, 20 mL) in a three-necked round flask (30 mL) was kept at desired temperature for 20 minutes, O_2 gas was babbled for 5 minutes. Oxygenations were completed within 10 to 20 minutes. Rate constants for decompositions of **2-R** were determined by monitoring decrease of the absorbance at 700 nm (see Figure S3 and Table S1). Deviations of the experimental data were estimated within ±10%.

X-ray crystallography. X-ray diffraction studies for $[Fe_2(OH)_2(H\text{-}L)]$-$(CF_3SO_3)_2\cdot0.5CH_2Cl_2\cdot0.5H_2O$ (**1**-H) and $[Fe_2(OH)_2\{H(H\text{-}L\text{-}O)\}_2](CF_3SO_3)_4\cdot CH_3COCH_3$ (**3**-H) were made on a Rigaku/MSC Mercury diffractometer with graphite monochromated Mo-Kα radiation (λ = 0.71073 Å). A total of 720 oscillation images were collected. A first sweep of data was done using ω scans from –80.0 to 100.0° in 0.50° step, at χ = 45.0° and φ = 0.0°. A second sweep of data was made using ω scans from –80.0 to 100.0° in 0.50° step, at χ = 45.0° and φ = 90.0°. Crystal-to-detector distances were 35 mm and detector swing angles were 10° for **1**-H and **3**-H. Exposure rates were 25.0 and 40.0 sec/° for **1**-H and **3**-H, respectively. The data were corrected for Lorentz and polarization effects. Empirical absorption corrections were applied. The structures of **1**-H and **3**-H were solved by a direct method (SIR92[1]) and expanded using a Fourier technique.[2] The structures were refined by a full-matrix least-squares method by using the SHELXL 2014[3] (Yadokari-XG[4]) or teXsan crystallographic software package[5] (Molecular Structure Corporation). ORTEP views (50% probability) of the complex of **1**-H and **3**-H with a full numbering scheme of atoms are shown in Figures S1 and S2. Selected bond distances (Å) and angles (deg) for **1**-H and **3**-H are listed in Tables S1 and S2. The crystallographic data and tables of final atomic coordinates, thermal parameters, and full bond distances and angles are given in CIF (CCDC 1430633 and 1430634).

[1] *SIR92*: A. Altomare, G. Cascarano, C. Giacovazzo, A. Guagliardi, M. C. Burla, G. Polidori, M. Camalli, *J. Appl. Crystallogr*. **1994**, *27*, 435.
[2] P. T. Beurskens, G. Admiral, G. Beurskens, W. P. Bosman, R. de Gelder, R. Israel, J. M. M. Smits, *The DIRDIF-94 program system (1994)*, Technical Report of the Crystallography Laboratory, University of Nijimegen, The Netherlands.
[3] G. M. Sheldrick, SHELXL-2014; G. M. Sheldrick, *Acta. Crystallogr.* **2008**, A64, 112.
[4] Yadokari-XG, Software for Crystal Structure Analyses, K. Wakita (2001); Release of Software Yadokari-XG (2009) for Crystal Structure Analyses, C. Kabuto, S. Akine, T. Nemoto, and E. Kwon, *J. Cryst. Soc. Jpn.*, **2009**, *51*,218.
[5] teXsan: *Crystal Structure Analysis Package*, Molecular Structure Corporation (1985 & 1992)

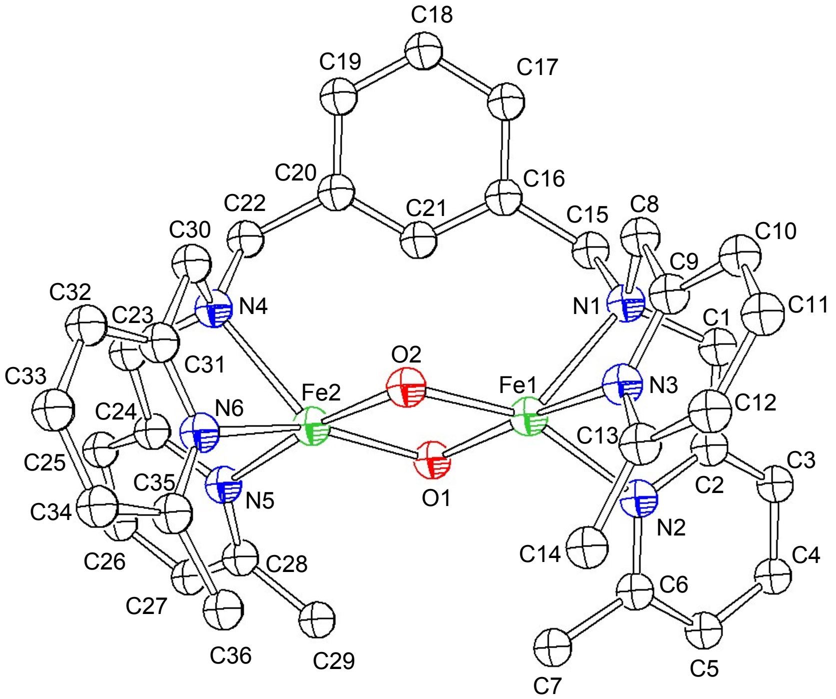

Figure S1. An ORTEP view of $[Fe_2(OH)_2(H\text{-}L)]^{2+}$ (**1**-H) with a full numbering scheme of atoms. Hydrogen atoms are omitted for clarity.

Table S1. Selected bond distances (Å) and angles (deg) of **1**-H.

Distances (Å)

Fe1–O1	2.013(2)	Fe2–O2	2.016(2)
Fe1–O2	1.976(3)	Fe2–N4	2.224(3)
Fe1–N1	2.216(3)	Fe2–N5	2.215(3)
Fe1–N2	2.185(3)	Fe2–N6	2.177(3)
Fe1–N3	2.225(3)	Fe1•••Fe2	3.0770(7)
Fe2–O1	1.986(2)		

Angles (deg)

O1–Fe1–O2	79.34(10)	N4–Fe2–N6	74.9(1)
O1–Fe1–N1	117.3(1)	N5–Fe2–N6	95.6(1)
O1–Fe1–N2	92.0(1)	Fe1–O1–Fe2	100.6(1)
O1–Fe1–N3	166.22(10)	Fe1–O2–Fe2	100.9(1)
O2–Fe1–N1	121.8(1)	Fe1–N1–C1	108.3(2)
O2–Fe1–N2	159.0(1)	Fe1–N1–C8	103.8(2)
O2–Fe1–N3	91.0(1)	Fe1–N1–C15	115.7(2)
N1–Fe1–N2	79.2(1)	Fe1–N2–C2	114.3(2)
N1–Fe1–N3	76.1(1)	Fe1–N2–C6	126.2(2)
N2–Fe1–N3	93.8(1)	Fe1–N3–C9	113.0(2)
O1–Fe2–O2	79.04(10)	Fe1–N3–C13	128.4(2)
O1–Fe2–N4	130.6(1)	Fe2–N4–C22	118.7(2)
O1–Fe2–N5	96.6(1)	Fe2–N4–C23	106.7(2)
O1–Fe2–N6	153.6(1)	Fe2–N4–C30	102.1(2)
O2–Fe2–N4	110.2(1)	Fe2–N5–C24	113.8(2)
O2–Fe2–N5	172.1(1)	Fe2–N5–C28	127.4(2)
O2–Fe2–N6	85.8(1)	Fe2–N6–C31	113.0(2)
N4–Fe2–N5	77.7(1)	Fe2–N6–C35	127.6(2)

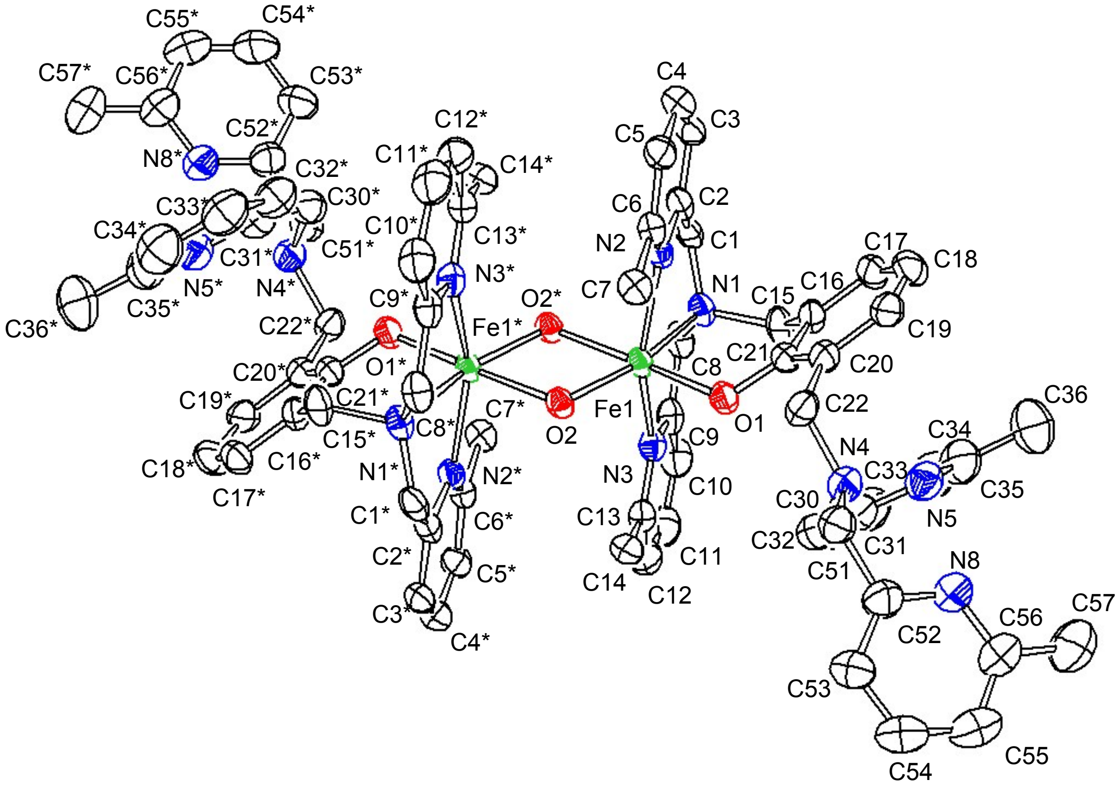

Figure S2. An ORTEP view of $[Fe_2(OH)_2\{H(H\text{-}L\text{-}O)\}_2]^{4+}$ (**3**-H) with a full numbering scheme of atoms. Hydrogen atoms are omitted for clarity.

Table S2. Selected bond distances (Å) and angles (deg) of **3**-H.

Distances (Å)			
Fe1–O1	1.902(3)	Fe1–N2	2.199(3)
Fe1–O2	1.938(3)	Fe1–N3	2.203(3)
Fe1–O2*	2.024(3)	Fe1•••Fe1*	3.156(1)
Fe1–N1	2.159(3)		

Angles (deg)			
O1–Fe1–O2	101.78(11)	O2*–Fe1–N2	91.13(11)
O1–Fe1–O2*	176.03(11)	N1–Fe1–N2	76.86(12)
O2–Fe1–O2*	74.42(12)	O1–Fe1–N3	91.63(12)
O1–Fe1–N1	94.24(12)	O2–Fe1–N3	101.18(12)
O2–Fe1–N1	163.93(12)	O2*–Fe1–N3	90.24(12)
O2*–Fe1–N1	89.60(11)	N1–Fe1–N3	76.77(13)
O1–Fe1–N2	88.75(12)	N2–Fe1–N3	153.58(12)
O2–Fe1–N2	104.59(12)	Fe1–O2–Fe1	105.58(12)

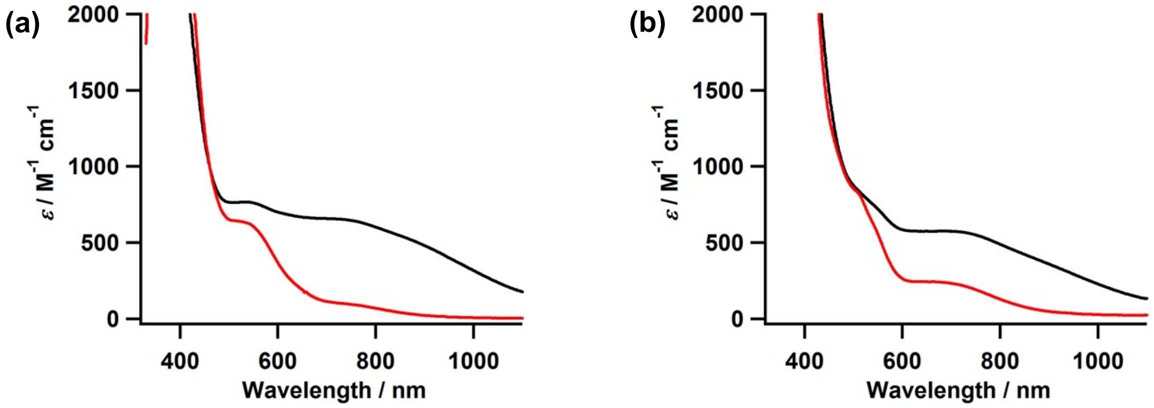

Figure S3. Electronic spectra of (a) **2**-tBu (black) and its decomposition species (red) (b) **2**-NO_2 (black) and its decomposition species (red) in acetone at –20˚C.

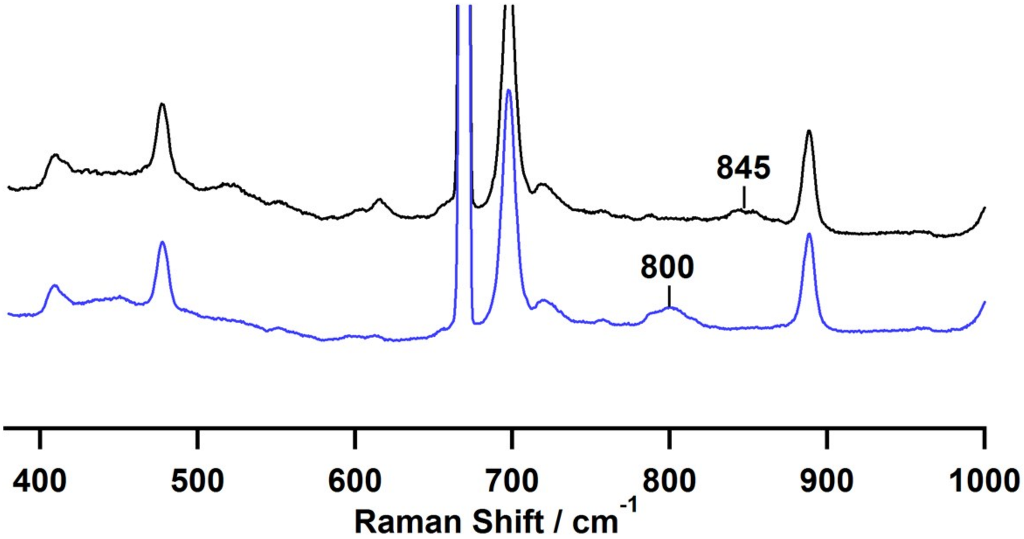

Figure S4. Resonance Raman spectra of **2**-H generated in the reaction of **1**-H with $^{16}O_2$ (black) and $^{18}O_2$ (blue) in d_6-acetone at –40 ˚C with a 647.1 nm laser excitation.

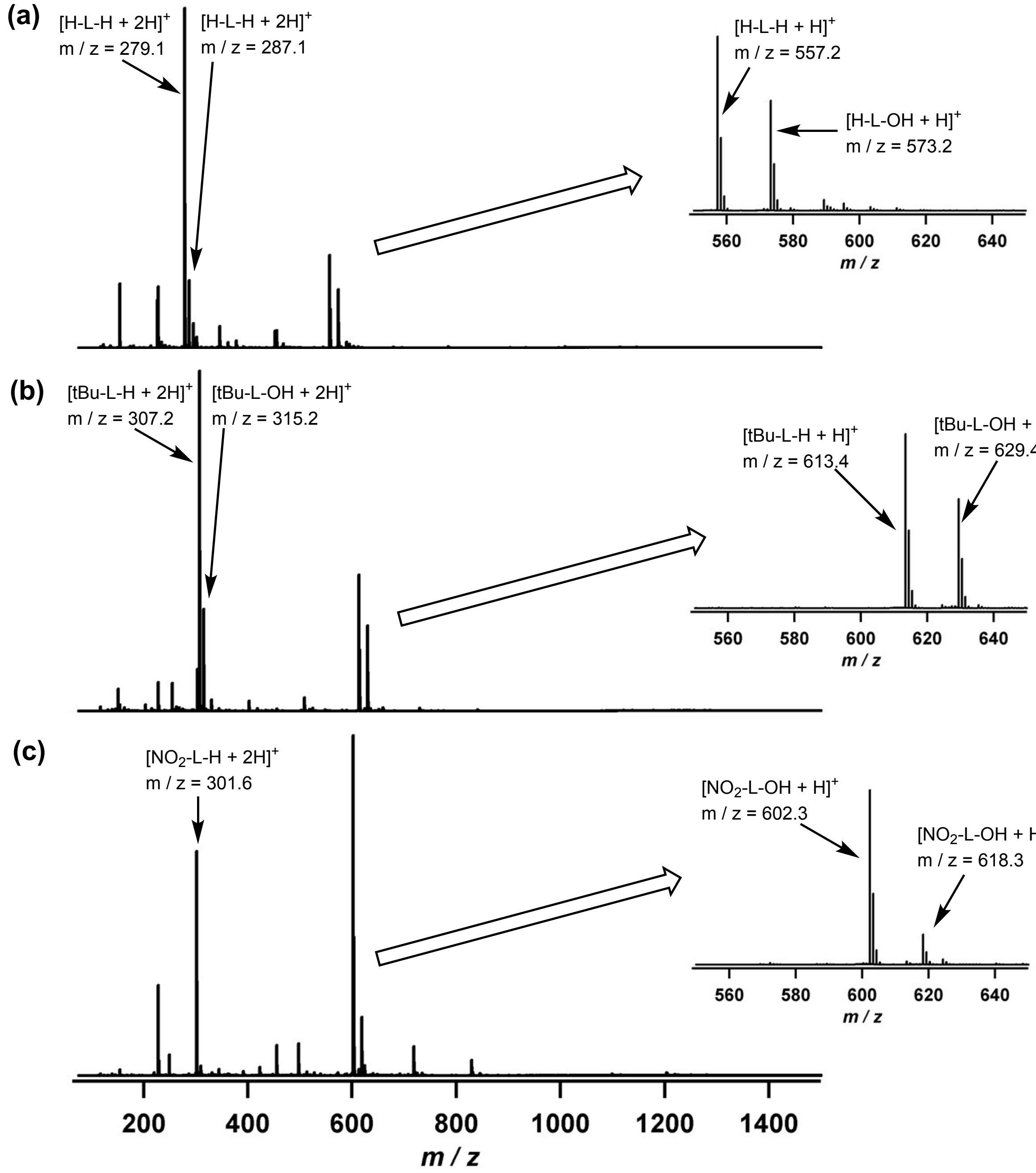

Figure S5. ESI-TOF mass spectra of samples obtained by the decomposition of (a) **2**-H, (b) **2**-tBu, and (c) **2**-NO_2.

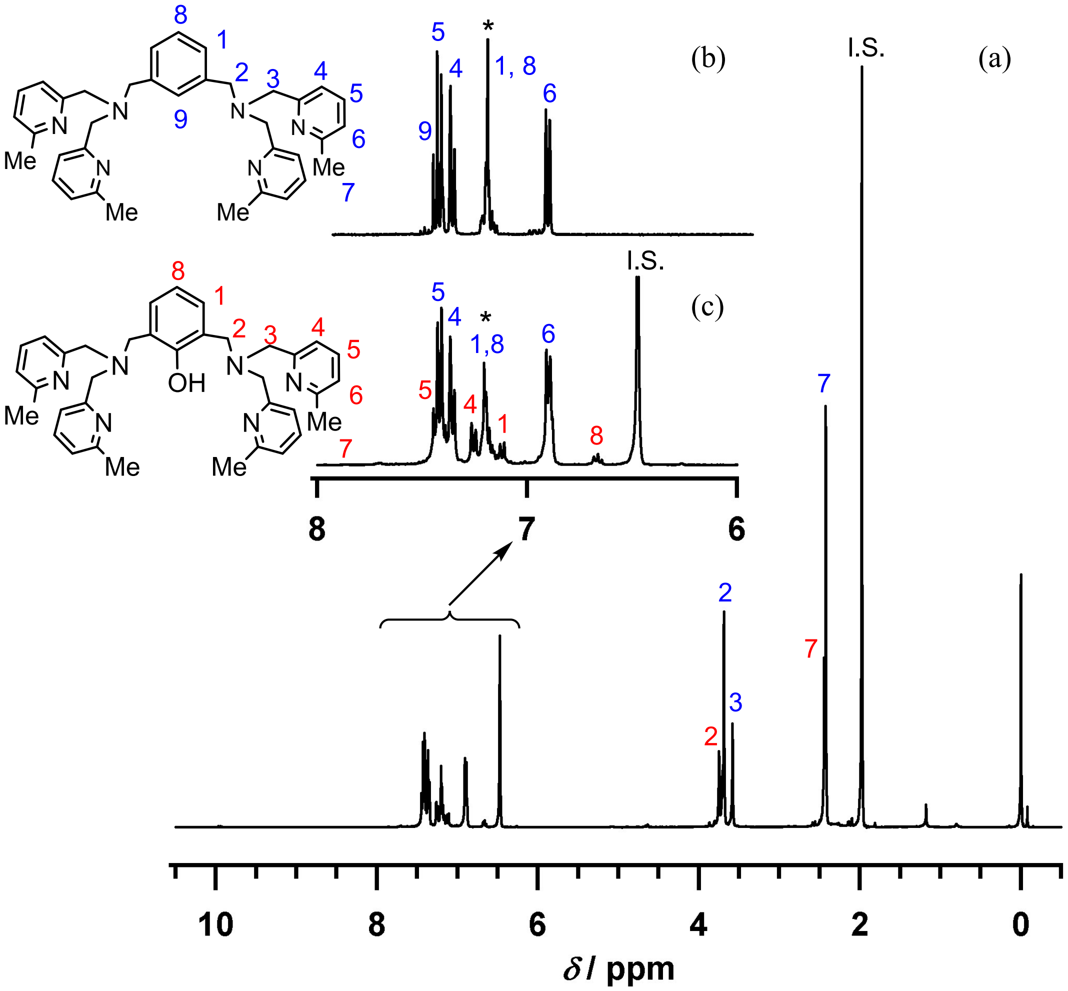

Figure S6. NMR specta of (a) a sample obtained by the decomposition of **2**-H, (c) its 6 – 8 ppm region, (b) H-L-H in 6 – 8 ppm region in $CDCl_3$. IS is an internal standard (2,6-dimetyl-1,4-benzoquinone). The asterisked signal is $CHCl_3$. Yield of H-L-OH was estimated by the average values obtained by comparison of the integrated area of the signals of 8, 4, and 1 with that of IS.

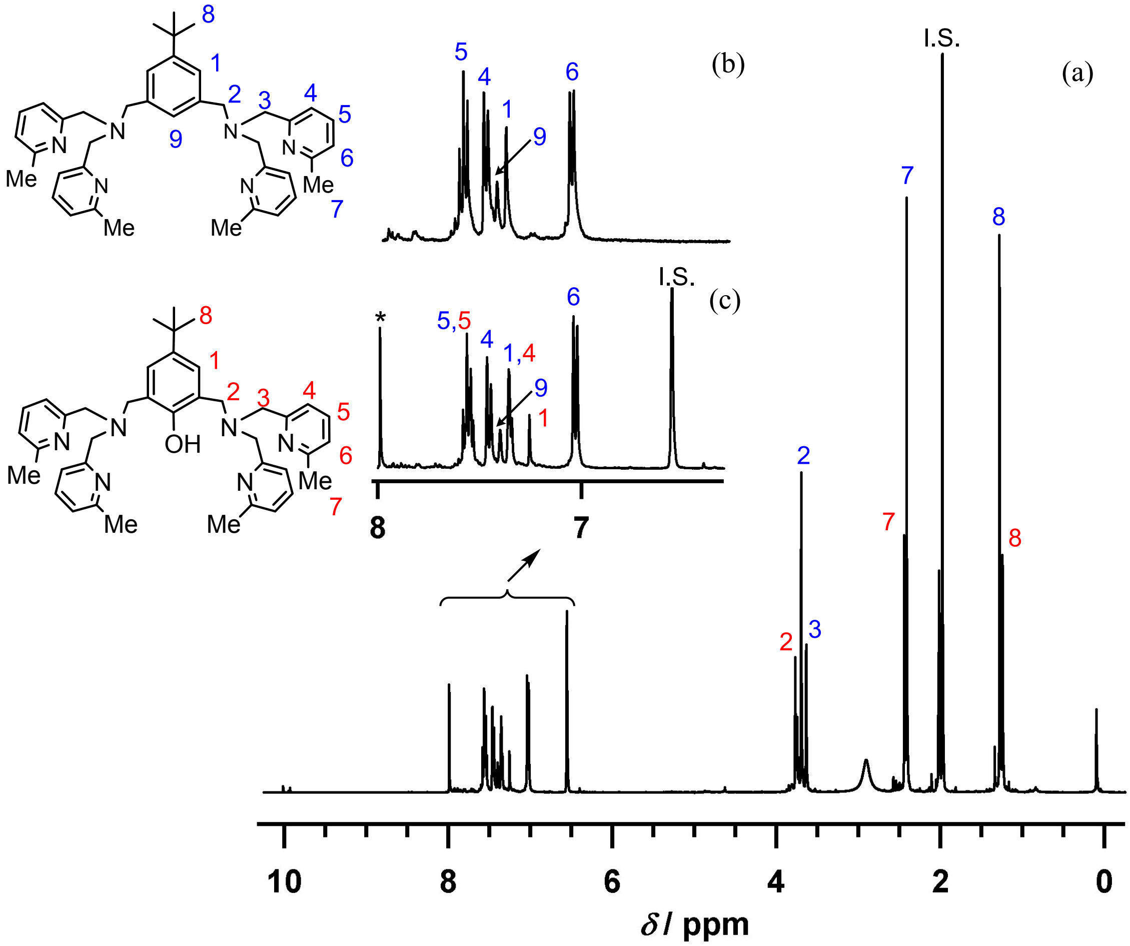

Figure S7. NMR specta of (a) a sample obtained by the decomposition of **2**-*t*Bu, (c) its 6 – 8 ppm region, (b) *t*Bu-L-H in 6 – 8 ppm region in acetone-d_6. IS is an internal standard (2,6-dimetyl-1,4-benzoquinone). The asterisked signal is $CHCl_3$. Yield of *t*Bu-L-OH was estimated by the average values obtained by comparison of the integrated area of the signals of 8, 4, and 1 with that of IS.

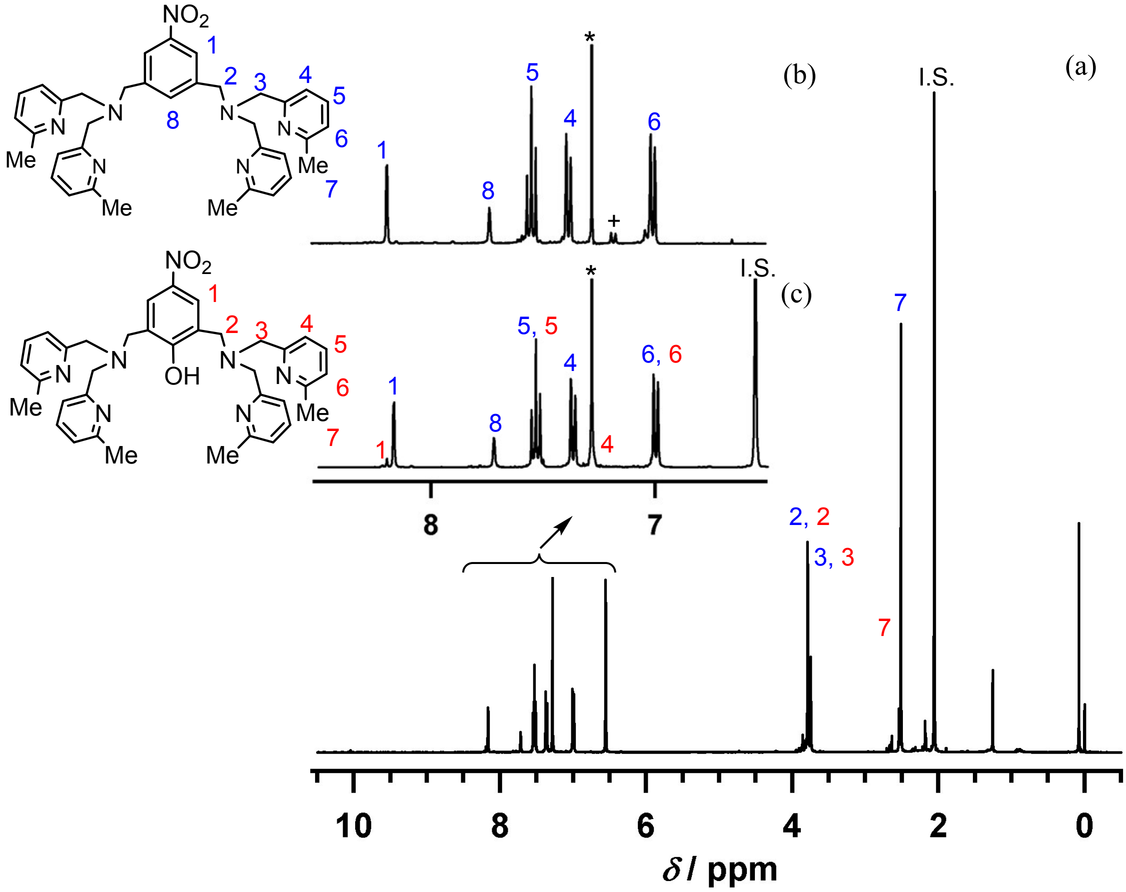

Figure S8. NMR specta of (a) a sample obtained by the decomposition of **2**-NO_2, (c) its 6.5 – 8.5 ppm region, (b) NO_2-L-H in 6.5 – 8.5 ppm region in $CDCl_3$. IS is an internal standard (2,6-dimetyl-1,4-benzoquinone). The asterisked signal is $CHCl_3$. Yield of NO_2-L-OH was estimated by the average values obtained by comparison of the integrated area of the signals of 8, 4, and 1 with that of IS.

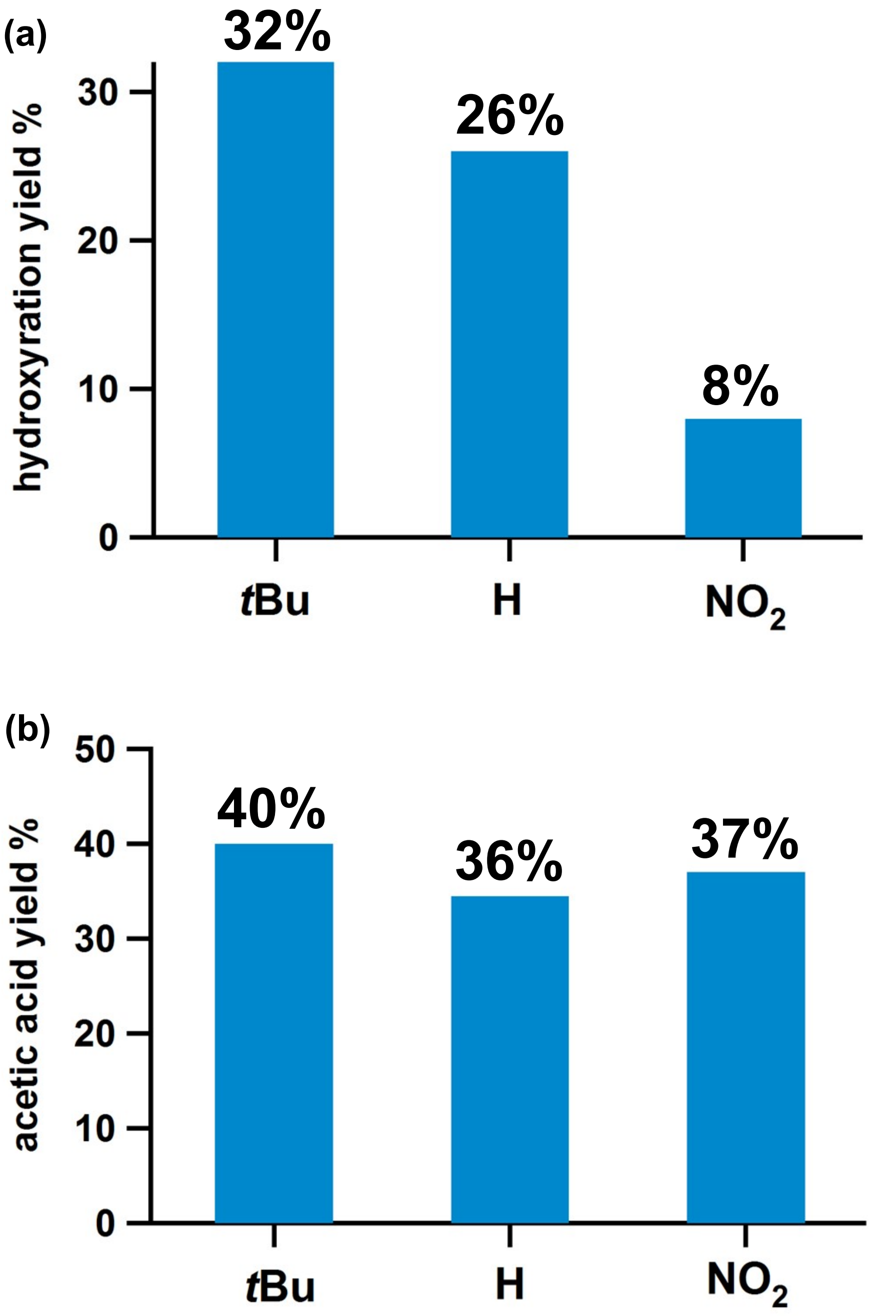

Figure S9. Yield of (a) hydroxylated ligands (tBu-L-OH, H-L-OH, and NO_2-L-OH) and (b) acetic acid.

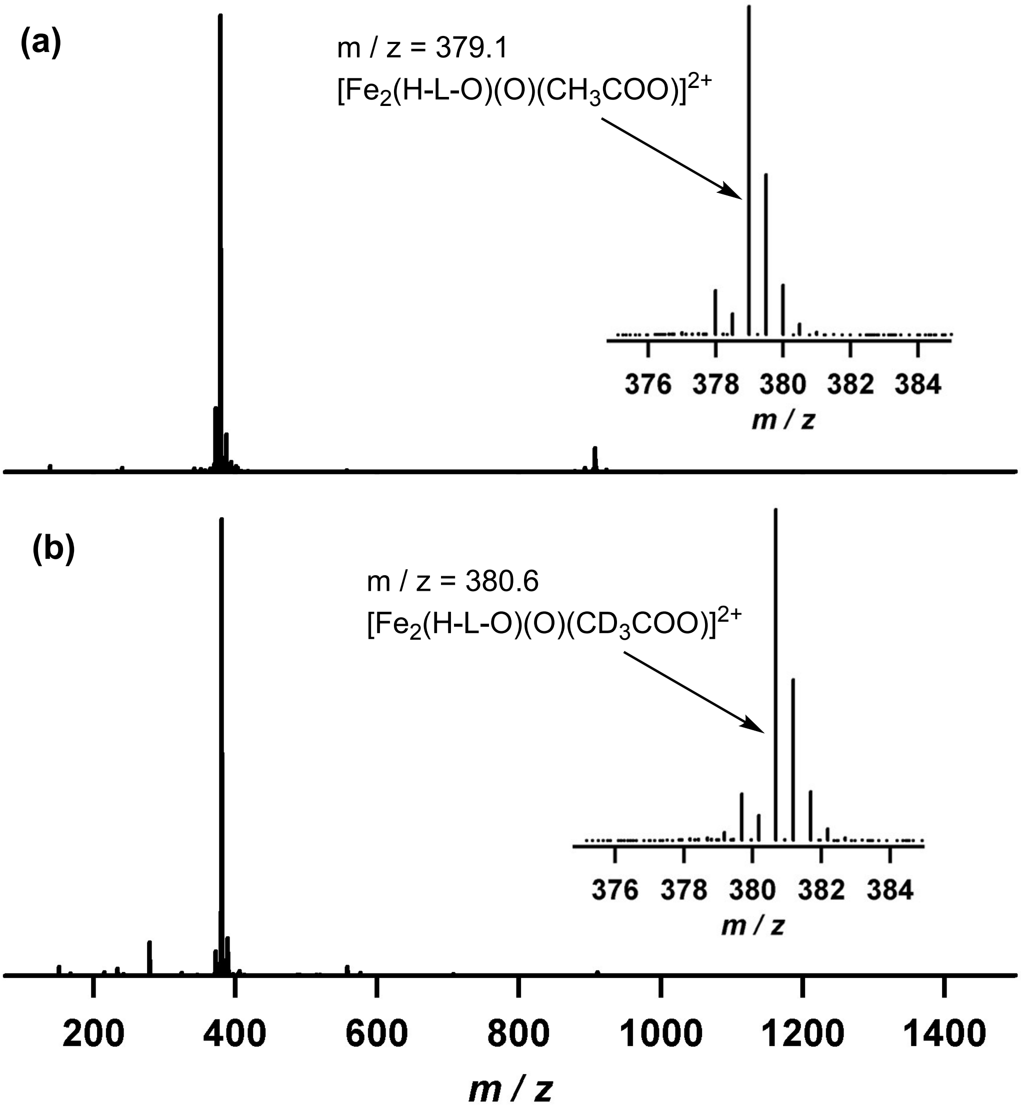

Figure S10. ESI-TOF mass spectra of red solution decomposed by **2**-H in (a) acetone and (b) d_6-acetone at −20 °C.

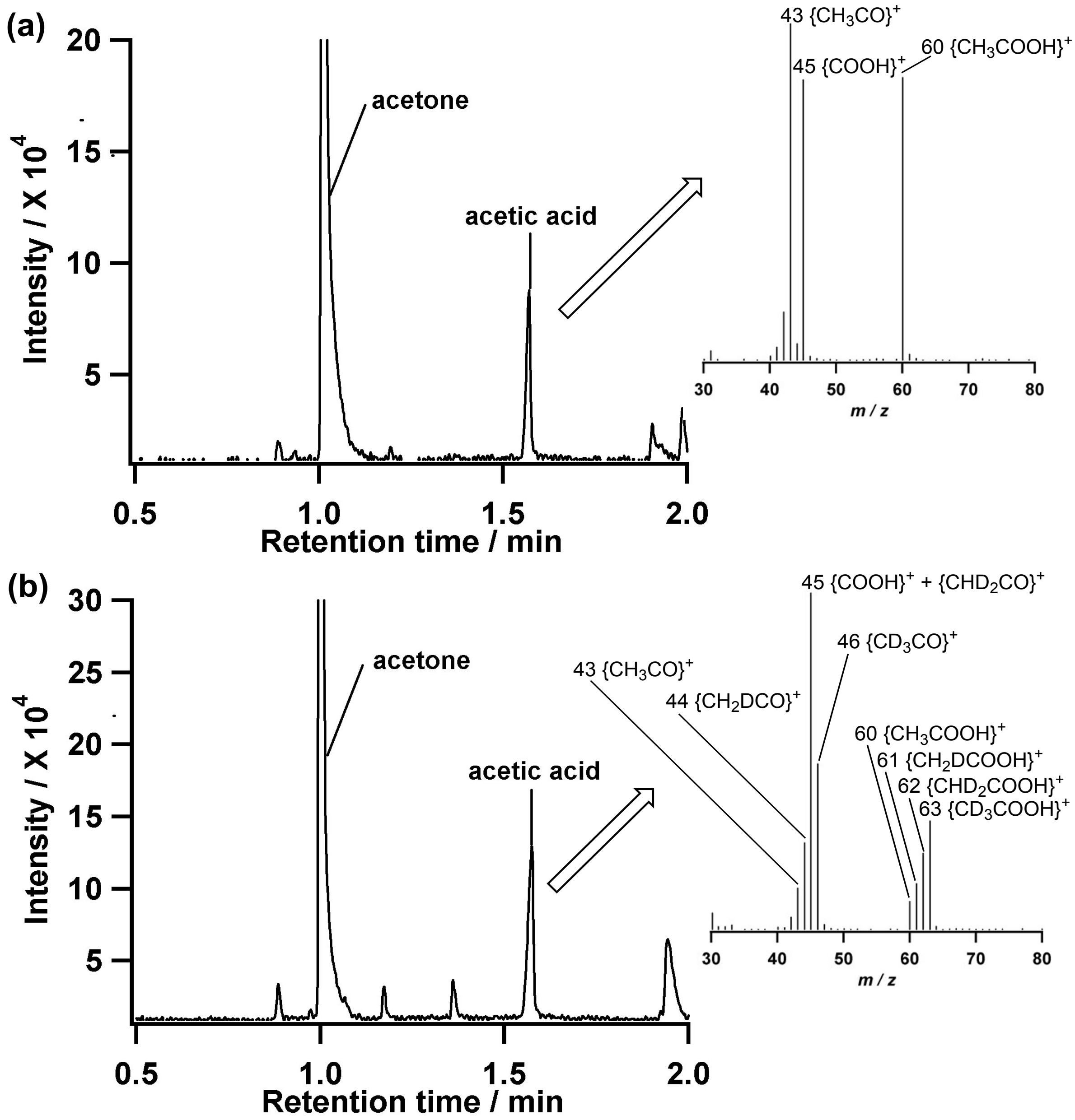

Figure S11. GC-mass spectra of acetic acid obtained in the decomposition of **2**-H in (a) acetone and (b) d_6-acetone.

(a) [**2**-H] =1.14 mM at –20 ºC

Time interval 1800 sec

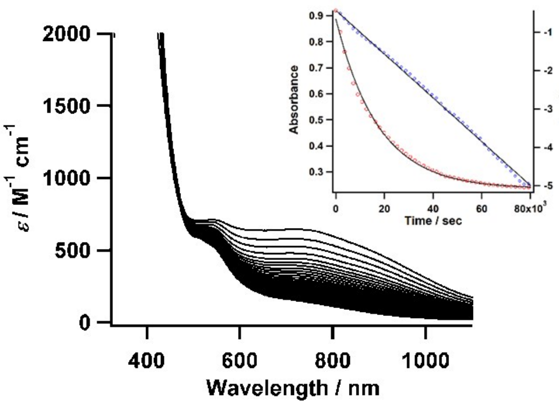

(b) [**2**-*t*Bu] = 1.44 mM at –20 ºC

Time interval 1800 sec

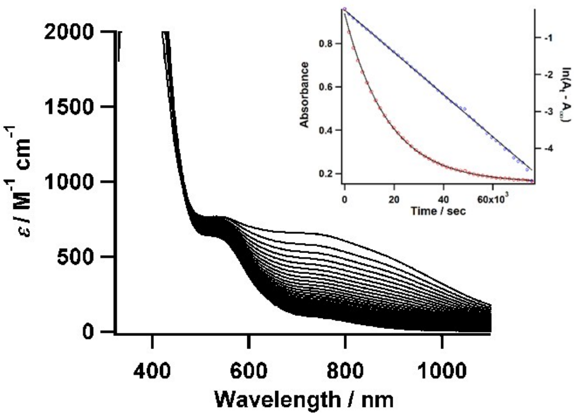

(c) [**2**-NO$_2$] = 1.02 mM at –20 ºC

Time interval 1800 sec

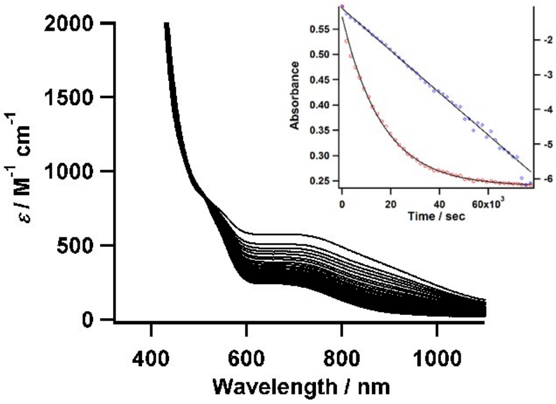

(d)

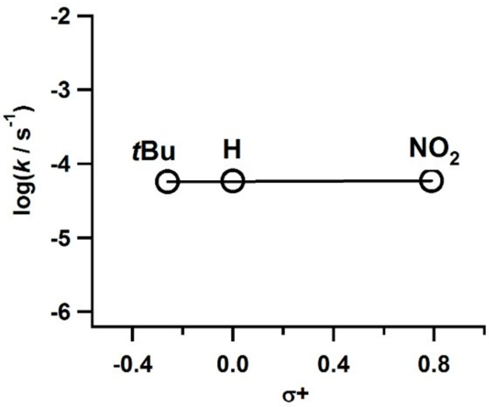

Figure S12. Representative electronic spectral changes for decompositions of (a) **2**-H ([**2**-H] = 1.14 mM), (b) **2**-*t*Bu ([**2**-*t*Bu] = 1.44 mM), and (c) **2**-NO$_2$ ([**2**-NO$_2$] = 1.02mM) in acetone at −20 °C. Insets are the decay-time profile of the absorbance at 700 nm (curve) and the pseudo-first-order plot (linear plot). (d) Hammet plot for the decomposition of **2**-R in acetone at −20 °C. Solid line represents a least square fit with the slope $\rho = 0.014$.

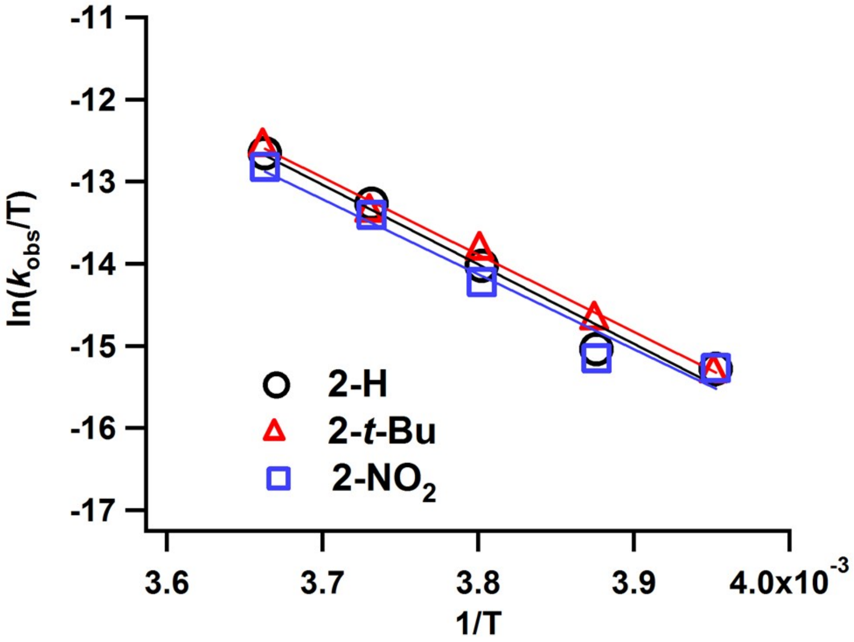

Figure S13. Eyring plots for decompositions of **2**-R (R = H, *t*Bu, and NO$_2$) in acetone.

Table S3. The first order rate constants (*k*) for the decomposition reactions of **2**-R (R = H, *t*Bu, and NO$_2$) in acetone. Deviation of the *k* value were estimated within 10%.

	2-H	**2**-*t*Bu	**2**-NO$_2$
T / K	*k* / s^{-1}	*k* / s^{-1}	*k* / s^{-1}
253	5.9×10^{-5}	5.7×10^{-5}	5.9×10^{-5}
258	7.6×10^{-5}	1.1×10^{-4}	6.8×10^{-5}
263	2.1×10^{-4}	2.6×10^{-4}	1.8×10^{-4}
268	4.6×10^{-4}	4.3×10^{-4}	3.9×10^{-4}
273	8.7×10^{-4}	9.9×10^{-4}	7.8×10^{-4}

Table S4. Kinetic activation parameters for the decomposition reactions of **2**-R (R = H, *t*Bu, and NO$_2$) in acetone.

Complex	$\Delta H^{‡}$ /kJ mol^{-1}	$\Delta S^{‡}$ /J mol^{-1} K^{-1}	*k* / s^{-1} (at −20 °C)
2-H	80	−8	5.9×10^{-5}
2-*t*Bu	78	−15	5.7×10^{-5}
2-NO$_2$	76	−26	5.9×10^{-5}

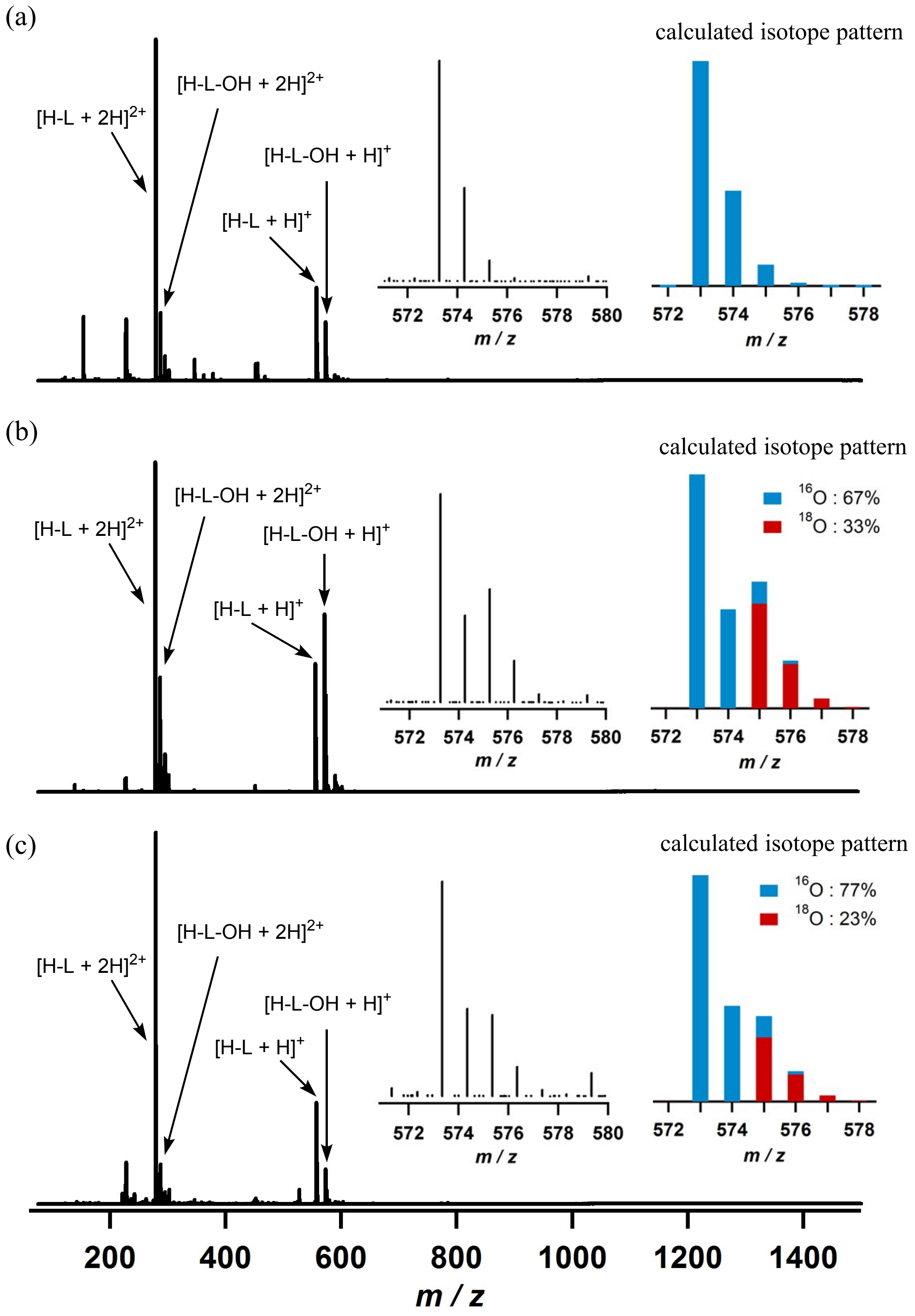

Figure S14. ESI-TOF mass spectra of (a) a sample obtained by the decomposition of **2**-H prepared from $^{16}O_2$, (b) a sample obtained by the decomposition of **2**-H prepared from $^{18}O_2$, and (c) a sample obtained by the decomposition of **2**-H prepared from $^{16}O_2$ in the presence of 1000 eqiv. of $H_2{}^{18}O$ at −20 °C.